Journal of Non-Crystalline Solids 624 (2024) 122722

Contents lists available at ScienceDirect

Journal of Non-Crystalline Solids

journal homepage: www.elsevier.com/locate/jnoncrysol

On the tool wear mechanism of machining Zr-based bulk metallic glasses under varying corner radii

Junsheng Zhang [a,b], Rang Li [a], Libao Zhang [a], Haidong Yang [a,*], Huohong Tang [a], Shunhua Chen [a,*]

[a] School of Mechanical Engineering, Hefei University of Technology, Hefei 230009, China
[b] Key Laboratory of Advanced Functional Materials and Devices of Anhui Province, Hefei University of Technology, Hefei 230009, China

ARTICLE INFO

Keywords:
Bulk metallic glass
Tool wear mechanism
Corner radius
Normal stress field
Machined surface morphology

ABSTRACT

Revealing the tool wear mechanisms of machining Zr-based bulk metallic glasses (BMGs) is important for the processing of BMGs in engineering applications. The tool wear mechanisms of machining BMGs with PCBN tools under varying corner radii were investigated, and the results shown that the adhesive and oxidation wear were the main wear mechanisms. The low thermal conductivity of the BMG workpiece material increased the cutting temperature. The effect of corner radius on tool wear mechanism was characterized by the normal stress fields. It indicated that the extremely high maximum normal stress was the main reason for edge chipping. Finally, the influence of tool wear state on machined surface quality was related to the machined surface morphology. The findings have shown that the edge chipping and adhesive wear produced feed marks, material side flow and adhensions on the machined surface, leading to the increase of surface roughness.

1. Introduction

Different form traditional crystalline alloys, bulk metallic glasses (BMGs) show excellent physical and chemical properties due to the absence of crystal defects, such as grain boundaries and dislocations, having broad application prospects in aerospace, military and medical equipment fields. Achieving desirable machining process is essential in order to realize their engineering applications. BMGs have exhibited excellent machinability with good surface roughness [1]. However, the cutting temperature is relatively high during machining, which lead to the appearance of light emission, surface crystallization and serious tool wear [2,3].

For the machining of BMGs, serious tool wear often occurs due to the high hardness, high strength and low thermal conductivity, which has then attracted a great deal of research attention. For example, the wear behavior was different for different tool materials due to the varied strength, hardness, wear resistance, and chemical stability. The tool wear of the cemented carbide tool with chemical vapor deposition coatings (WC-CVD), polycrystalline cubic boron nitride (PCBN) and polycrystalline diamond (PCD) tools during the turning of BMGs was compared [4]. Serious chip welding occurred on the tool nose when machining using the WC-CVD tool. For PCBN and PCD tools, minor chipping at the cutting edge was observed, caused by the impact during cutting. The surface roughness, chip morphology and tool wear behavior during the machining of Fe-based BMG overlay using TiAlN coated inserts was also analyzed [5]. The results showed that the wear mechanism of TiAlN coated insert was a comprehensive process, including abrasion, adhesion, fatigue and chipping. The ultra-precision cutting of BMGs can be achieved with the diamond tool and PCBN tool [6]. Different from the excellent chemical resistance of PCBN tool, the diamond tool presented higher chemical affinity with Zr of the workpiece material during micro-machining. The adhesion wear and machined surface quality of PCBN tool were better than those using diamond tool. The wear mechanism of single-point diamond tools during the machining of the $Pd_{40}Ni_{10}Cu_{30}P_{20}$ BMG was then discussed [7]. The built-up edge was formed on the cutting edge, which was mainly due to the high elasticity and viscosity of workpiece material. Thereafter, the thermo-mechanical coupled wear behavior evolution of cemented carbide inserts was presented in the machining of Zr-based BMGs [8]. The chip adhesion covered the rake and flank surface, led to adhesive wear on the cutting edge, and changed the actual rake angle of the insert.

On the other hand, the cutting parameters and processing methods also have significant influence on tool wear behavior of BMGs. A case in point, the influence of cutting parameters on tool wear in drilling BMG

* Corresponding authors.
E-mail addresses: yanghaidonghfut@126.com (H. Yang), shchen@hfut.edu.cn (S. Chen).

https://doi.org/10.1016/j.jnoncrysol.2023.122722
Received 1 August 2023; Received in revised form 10 October 2023; Accepted 31 October 2023
Available online 6 November 2023

was examined [9]. At high spindle speed, the temperature was high associated with light emission and severe tool wear. It was found that the tool wear was the main reason for the light emission phenomenon during the high-speed cutting of Zr-based BMG [10]. The front chamfer would generate the accumulation of chips, leading to the increase of adhesive wear and light emission. The better wear resistance and anti-adhesion ability of insert were beneficial for reducing the friction characteristics of tool-chip interface and suppressing the appearance of light emission. During the high-speed milling of Zr-based BMGs, adhesion wear was the dominant mechanism of flank wear [11]. The introduction of mist coolant can effectively suppress the appearance of light emission and reduce the tool wear about 70 %. The machinability of Zr-based BMG during micro milling can also be characterized with tool wear [12]. Compared with the machining of Al6061, the tool wear of Zr-based BMG was more stable after milling 300 mm, and only slight chipping and abrasive wear were found on the cutting edge. The ultrasonic vibration was also applied in the machining of Zr-based BMG [13]. The increase of ultrasonic amplitude can increase the cutting-in speed between the tool and workpiece, leading to severe abrupt fracture. The actual cutting distance was also increased and the flank wear of insert would be enhanced in terms of abrasion.

In addition to the tool materials, cutting parameters and processing methods, the geometric parameters of insert such as corner radius also affect the tool wear behavior of BMGs [14–16]. Revealing the influence of corner radius on tool wear mechanism is beneficial for optimizing the machining process, and improving the tool life and surface quality. However, although some studies have paid attention to the tool wear behavior of machining BMGs, the internal mechanisms of how the tool wear behavior is affected by corner radius is not clear. And the way of tool wear state during the machining of BMGs, affecting the machined surface quality, also needs further investigations. In this work, an investigation on the tool wear mechanism of machining Zr-based BMGs was performed. The effect of corner radius on wear mechanism was analyzed carefully by considering the normal stress field distribution on the rake face. The influence of tool wear behavior on cutting performance, including cutting force, surface roughness, and machined surface morphology, was also investigated.

2. Methodology

$Zr_{57}Cu_{20}Al_{10}Ni_8Ti_5$ (at.%) BMG was selected as workpiece material in this research. The BMG bars with the diameter of 5 mm and length of 90 mm were prepared by arc melting method [17,18]. The microstructure was detected using X-ray diffraction (XRD) analysis to ensure the completely amorphous atomic structure [1]. In this work, the machined surfaces of BMGs would also be inspected by XRD. The physical and mechanical properties of the workpiece material are presented in Table 1.

PCBN inserts are widely used in the processing of super-hard material because of its high hardness, excellent wear resistance, high thermal stability, and excellent thermal conductivity. As previous research reported [4,6], PCBN tools showed excellent machinability and surface roughness during the machining of BMGs. The PCBN tool was also selected in this research, and the tool material compositions and partial physical properties are presented in Table 2.

Based on previous studies [1,17], the cutting depth a_p=0.2 mm and feed rate f = 0.039 mm/r are beneficial to improving the machined surface roughness. The cutting speed v_c=0.16 m/s was chosen because of the lathe speed limit and small diameter of the workpiece. In order to study the influence of corner radius on wear behavior, PCBN tools with different corner radii (0.4, 0.8, 1.2, and 1.6 mm) were prepared. The cutting parameters and tool geometric parameters are presented in Table 3.

Table 1
Physical and mechanical properties of the workpiece material.

Material	Yield strength (MPa)	Elastic modulus (GPa)	Thermal conductivity (W/m·K)	Hardness ($HV_{0.5}$)
$Zr_{57}Cu_{20}Al_{10}Ni_8Ti_5$	1635	82.0	7.1	537.3

Table 2
Tool material compositions and physical properties of PCBN tool.

Type	CBN content (vol%)	Binder	Thermal conductivity (W/m·K)	Hardness (HV)	Fracture toughness ($MPa·m^{0.5}$)
BN100	85	TiN/Co	217	3700–4000	0.8

The cutting process was conducted on a CA6140 lathe equipped with the three-dimensional dynamometer Kistler 9257B and the frequency converter 3G3RV-A4075-ZV, as shown in Fig. 1. The dynamometer was used to measure and record the cutting forces, i.e., *Fx, Fy*, and *Fz*, during machining. The sensitivity of *Fx, Fy*, and *Fz* can reach 7.5 pC/N, 7.5 pC/N, and 3.7 pC/N, respectively.

As the workpiece is a slender bar with diameter of 5 mm, it was clamped on left and supported by the top on right, to improve the stability of the process system. The BMG bars were then machined to standard size with a diameter of 4.6 mm to remove the surface oxide layer, and to ensure the roundness of workpiece before the tool wear experiment. The machining time is 10 min for each tool. The tool wear state was checked with a tool microscope during machining. After machining, the machined surface morphology and the PCBN tool rake and flank face morphologies were analyzed using scanning electron microscopy (SEM) and energy dispersive spectroscopy (EDS). The machined surface roughness was examined with JH-340 roughness tester.

3. Results and discussion

3.1. Tool wear morphology

Due to the excellent mechanical properties of BMGs, the tool wear has always been an important problem during its machining. Here, the wear behavior of BMGs with PCBN tools was investigated in detail. As shown in Fig. 2(a) and (b), edge chipping and adhesion were observed on the tool rake and flank faces at the corner radius of 0.4 *mm*. Due to the relatively-small corner radius, the tool-chip contact area was also small. The stress field on rake face was more concentrated at the cutting edge, which facilitated the appearance of edge chipping. Beside, with the low thermal conductivity (7.1 W/m·K) of the Zr-based BMG [1,8,17], large amount of cutting heat generated during machining is hard to dissipate, resulting in high temperature of tool-chip interface. Under the combined action of serious friction at the tool-chip interface and high temperature, the chip bottom material is continuously bonded to the tool rake face, forming adhesion. At the same time, due to the edge chipping, a newly flank face was exposed which decreased the tool clearance angle and destroyed the regular shape of cutting edge. The friction and extrusion between the tool-workpiece contact area were then increased, also

Table 3
The cutting parameters and tool geometric parameters.

Cutting parameters		Geometric parameters	
Cutting speed v_c	0.16 m/s	Rake angle γ_o	0°
cutting depth a_p	0.2 mm	Major cutting edge angle κ_r	90°
feed rate f	0.039 mm/r	Clearance angle α_o	7°
		Corner radius r_ε	0.4, 0.8, 1.2, 1.6 mm

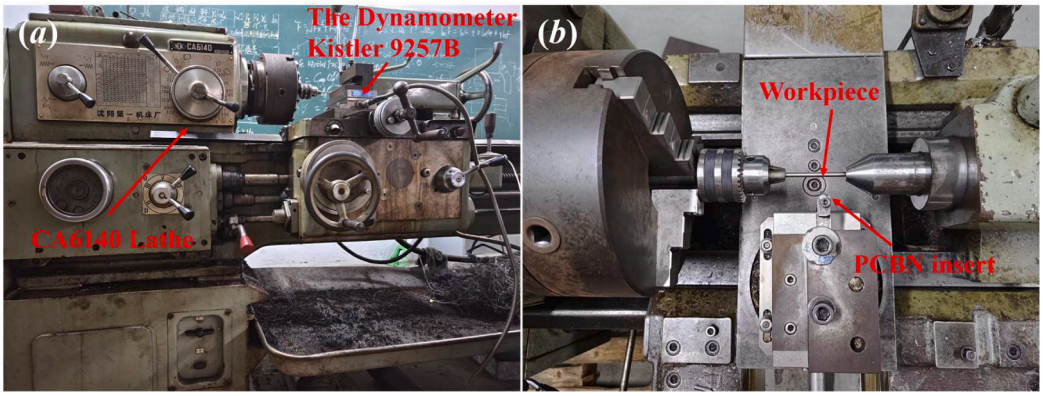

Fig. 1. (a) The experimental setup for machining, and (b) the installation of workpiece and cutting tool.

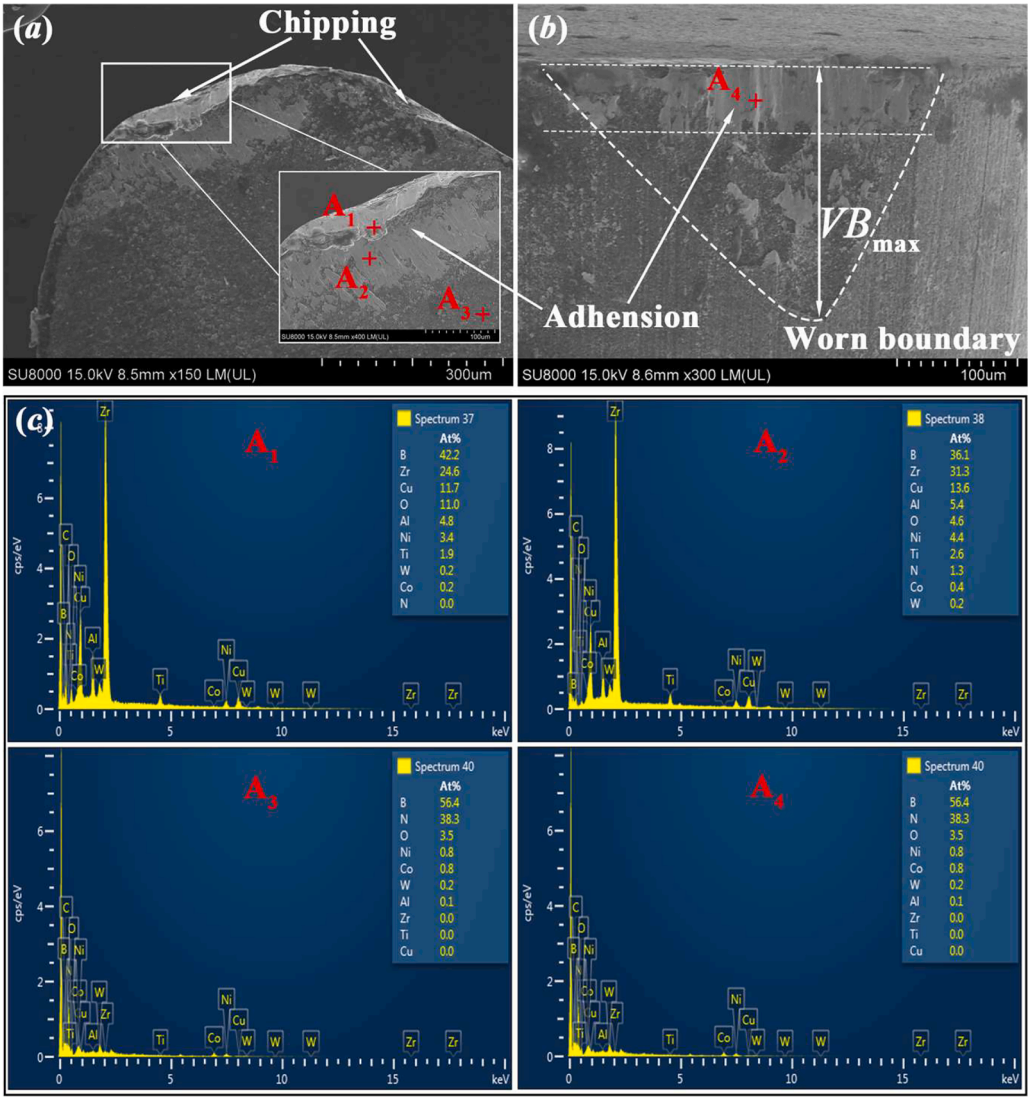

Fig. 2. (a) Rake face morphologies, (b) flank face morphologies, and (c) the EDS spectrum corresponding points (r_ε = 0.4 mm).

leading to the appearance of adhesion on the flank face.

Different from the tool wear state at corner radius of 0.4 mm, when the PCBN tool corner radius increased to 0.8 and 1.2 mm, the edge chipping phenomenon disappeared, adhesion and built-up edge occurred on the rake face. The tool-chip contact area increased with corner radius increasing from 0.4 to 0.8 and 1.2 mm. The degree of stress concentration decreased and the curvature of the tool tip became smaller. Thus, the strength of tool nose was relatively high and the edge chipping disappeared here. The adhesion on the rake face and flank face still existed, because of the inevitable friction between the cutting tool and chip or workpiece and the less adhesion on the flank face at the corner radius of 0.8 and 1.2 mm. It was mainly due to the integrity of

cutting edge, as shown in Figs. 3(a)–(d) and 4(a), (b), which can ensure good friction state at the tool-workpiece interface. Additionally, a lot of chip adhesives were observed on the main cutting edge. It indicated that the chip materials tended to stick to the cutting edge and form the built-up edge (BUE) because of the particular temperature and stress during machining. The appearance of built-up edge can protect the cutting edge partially from abrasion of hard particles. On the other hand, it will also fall off and reappear periodically, causing the variation of rake angle and cutting force.

With the tool corner radius increasing to 1.6 mm, the edge chipping and adhesion appeared again and the built-up edge disappeared, as shown in Fig. 5(a)–(d). Although the strength of tool nose increased with the increase of corner radius, the cutting force, especially the radial force, also increased at the same time. It enlarged the extrusion between the PCBN tool and workpiece material, and strengthened the impact of shock and vibration on the tool nose during machining. Although the PCBN tool has a series of characteristics, such as high hardness, high wear resistance and good thermal stability, its toughness and bending

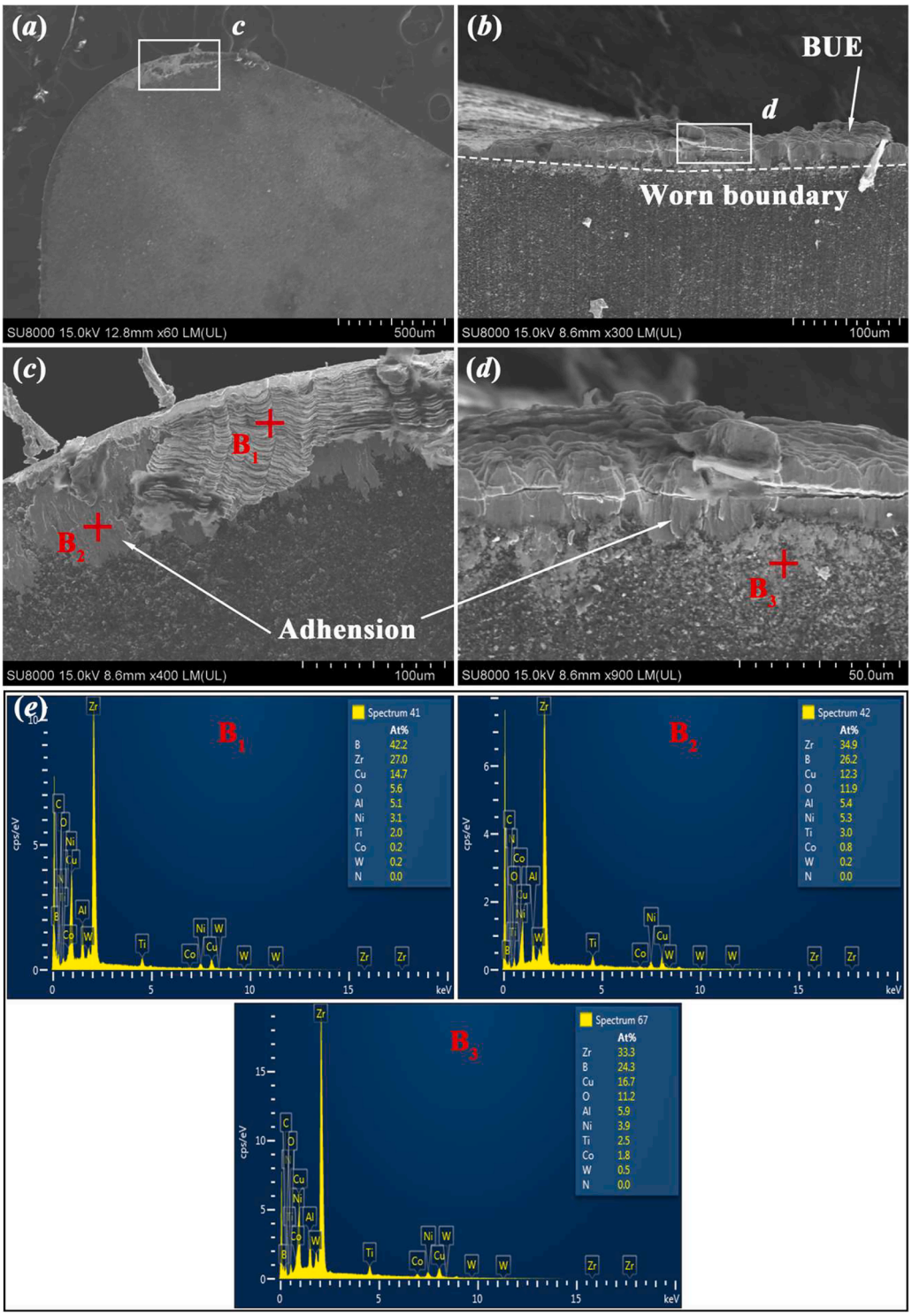

Fig. 3. (a) Rake face morphologies, (b) flank face morphologies, (c)-(d) detail enlarged view in rectangle region of (a) and (b) respectively, and (e) the EDS spectrum corresponding points ($r_\varepsilon = 0.8$ mm).

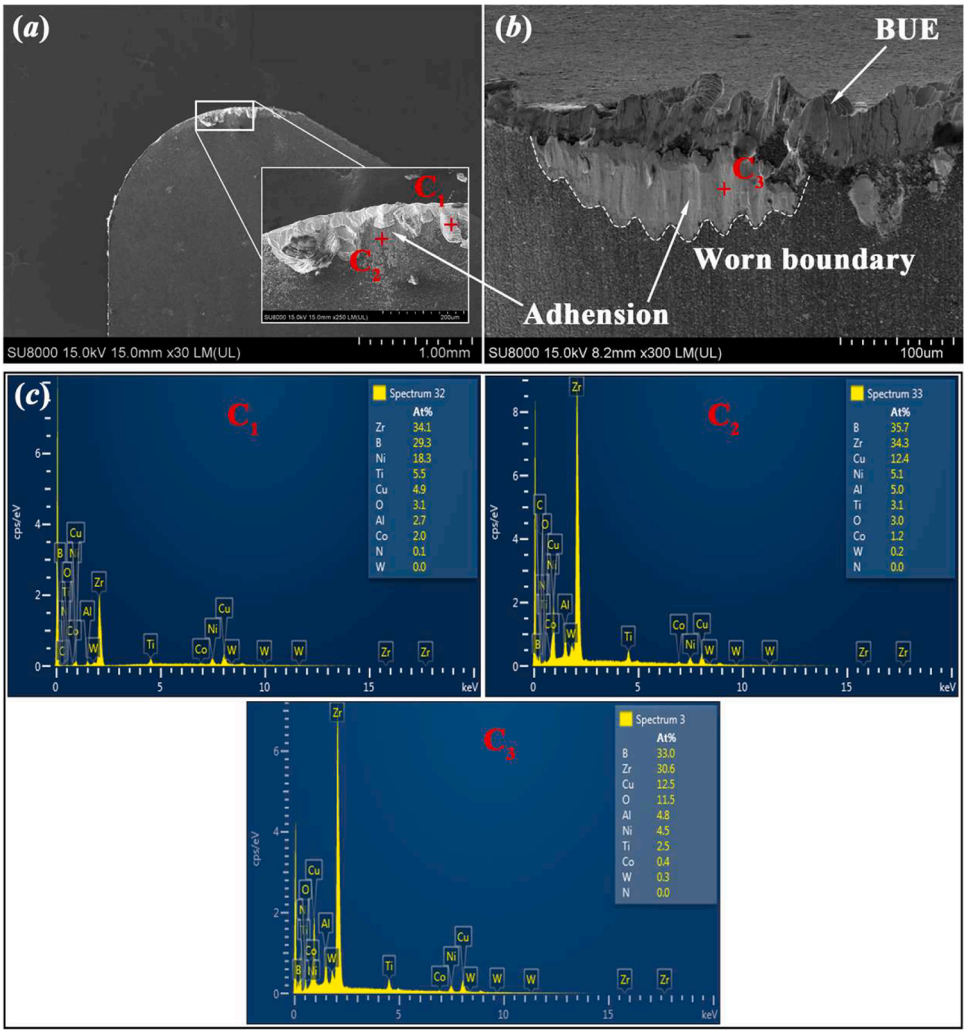

Fig. 4. (a) Rake face morphologies, (b) flank face morphologies, and (c) the EDS spectrum corresponding points (r_ε = 1.2 mm).

strength is poor, which is extremely sensitive to shock and vibration during cutting. As the most vulnerable part of the tool, the tool nose was subjected to the most complex thermal and mechanical shock. As a result, micro-chipping occurred on the main cutting edge. Therefore, the micro-chipped cutting edge without intact rake face was not conducive to chip bonding leading to the disappearance of built-up edge.

In general, the tool wear state of BMGs was stable and built-up edge appeared at the corner radius of 0.8 and 1.2 mm. A smaller corner radius would cause stress concentration, while a larger corner radius would strengthen the impact of shock and vibration during machining, both leading to the chipping of cutting edge. The adhesion on tool rake and flank faces always existed with the increase of corner radius, which was mainly influenced by the temperature. As the tool corner radius increased, the length of the cutting edge involved in cutting was also continuously growing, and the friction at the tool-workpiece interface continued to intensify, resulting in heat accumulation and cutting temperature increase. Therefore, the variation of corner radius may also be one of the reasons for the adhesion. But when the tool corner radius was 0.4 and 1.6 mm, the appearance of edge chipping would also reduce the adhesion.

3.2. Tool wear mechanism

The tool wear morphologies indicated that adhesion, built-up edge and edge chipping were the main wear behavior during the machining of the Zr-based BMG using PCBN tools. In order to analyze the wear mechanism, element distributions in the tool worn areas were detected using EDS. As presented in Fig. 6, a large amount of Zr element was found on the tool rake face, which was concentrated near to the tool nose. Beside, the concentration of Zr element was obvious at the corner radius of 0.4 mm, which would gradually decrease with the corner radius increasing to 1.6 mm. Here, since Zr was the main element of workpiece material, the appearance of Zr element indicated the existence of adhesive wear on the rake face. During machining, the tool-chip contact area will generate high temperature and pressure because of the friction and extrusion. The chip material will then be softened and stick to the rake face under particular temperature and pressure. As the temperature and pressure were relatively high near the tool nose, the adhesive wear also became more serious here.

Further analysis of the elements at the built-up edge was also conducted with the corner radii of 0.8 and 1.2 mm, as presented in Fig. 3(e), spectrum B_1 and Fig. 4(c), spectrum C_1. The appearance of large amount of Zr element confirmed that chip materials tended to stick and accumulate on the intact cutting edge. With the machining progressing, the built-up edge will appear and fall off periodically, leading to adhesive wear. Here, the concentration of Zr was mainly caused by the adhesion and built-up edge. When the corner radius increased to 1.6 mm, although large amount of Zr element was detected on the rake face, the concentration of Zr element was relatively small near to the tool nose. It may be caused by the micro-chipping of the cutting edge.

The adhesion existed not only on the rake face, but also on the flank face. Figs. 2–5 showed the element distribution of adhensions at

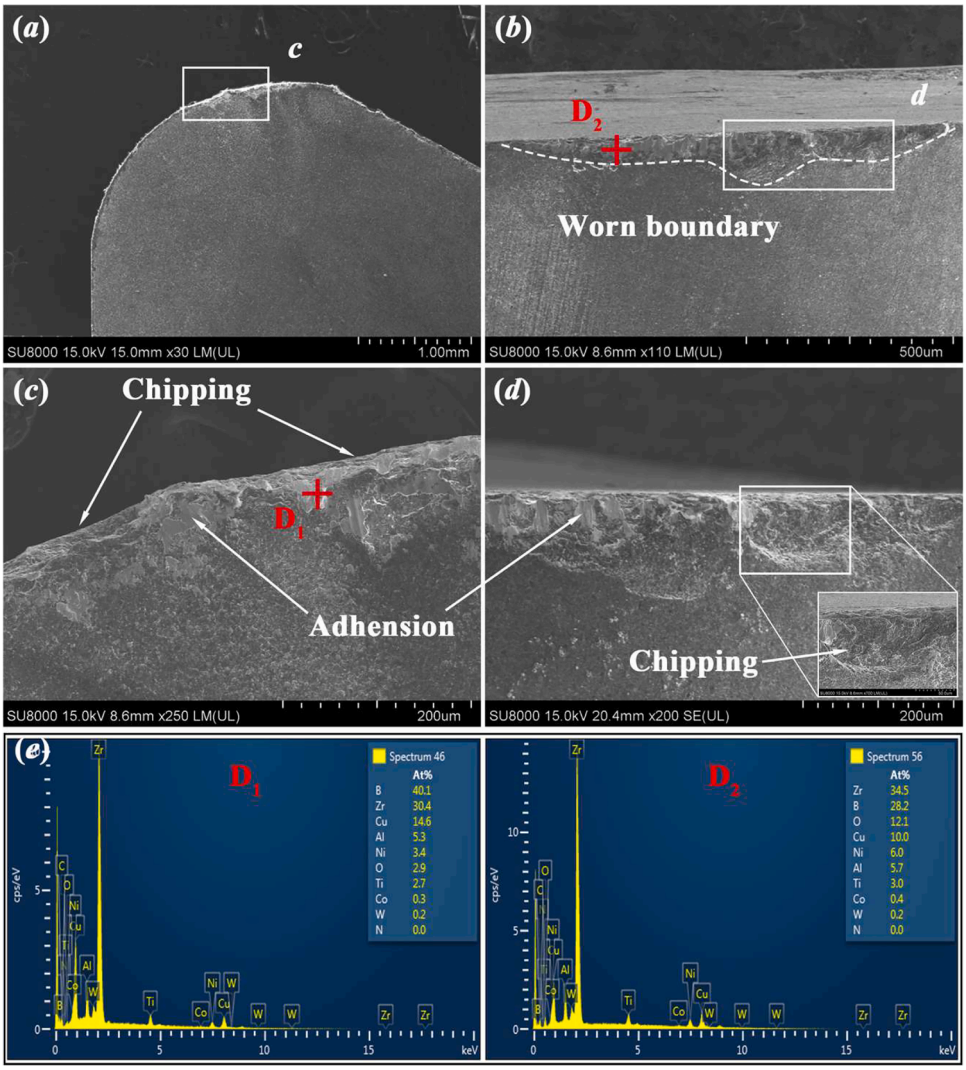

Fig. 5. (a) Rake face morphologies, (b) flank face morphologies, (c)-(d) detail enlarged view in rectangle region of (a) and (b) respectively, and (e) the EDS spectrum corresponding points ($r_\varepsilon = 1.6$ mm).

different corner radii, respectively. In spite of Zr, Cu, Al, Ni, and Ti elements which are the main element of workpiece material, large amount of B and small amount of O and Co element are also observed in the adhensions. B element is the main element of PCBN tool material and Co element comes from the binder of CBN particles. The N element, which is also the main element of PCBN tool material, almost disappeared in the adhesion area. The appearance of O element indicated the existence of oxidation reaction. As the low thermal conductivity of Zr-based BMGs, cutting heat was concentrated on the tool-chip contact area, leading to the local high temperature. The CBN particles in the tool and the Co element in the binder were easy to oxidize with O_2 in the air, forming B_2O_3, CoO and Co_3O_4. The chemical reaction can be expressed by [19,20]:

$$4BN + 3O_2 \rightarrow 2N_2\uparrow + 2B_2O_3 \quad (1)$$

$$2Co + O_2 \rightarrow 2CoO \quad (2)$$

$$3Co + 2O_2 \rightarrow Co_3O_4 \quad (3)$$

Finally, the product of the reaction will be mixed with the softened chip material, forming adhesion on the rake and flank faces. Therefore, a large amount of B element was detected in the adhensions, while the content of N element was very little since the N element escaped in the form of nitrogen. This process is presented in Fig. 7. Beside, the temperature near to the tool nose was relatively high, and the oxidation reaction was more serious here. This resulted in lower content of N element and higher O content, as presented in Fig. 2(c) (spectrum A_1, A_2 and A_3). Along with the oxidation reaction, the composition of the tool surface layer was changed, and its physical performance would also be destroyed. The tool wear behavior would be aggravated due to the presence of oxidation wear.

In conclusion, the adhesive wear and oxidation wear are the main wear mechanisms during machining Zr-based BMGs with PCBN tools. The high temperature and pressure caused by the friction and extrusion at the tool-chip and tool-workpiece interface are the main reason for adhesive wear. In addition, the high temperature also causes the CBN particles in the tool material and the Co element in the binder to react with oxygen in the air, leading to oxidation wear.

3.3. *Effect of normal stress field distribution on tool wear behavior*

As mentioned above, the tool wear was mainly caused by the high temperature and pressure at the tool-chip and tool-workpiece interface. Tool breakage, such as edge chipping, also occurred at the corner radii of 0.4 and 1.6 mm during the machining of Zr-based BMGs with PCBN tools. Here, the stress field distribution on the rake face has a direct influence on tool breakage. When the maximum normal stress at the tool nose is high enough, the edge chipping will be easy to occur. In order to

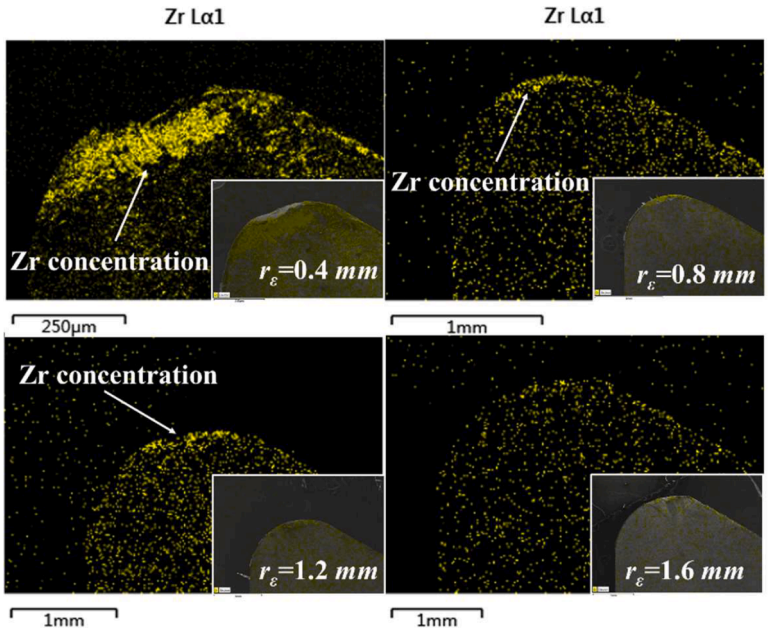

Fig. 6. The concentration of Zr element on the rake face.

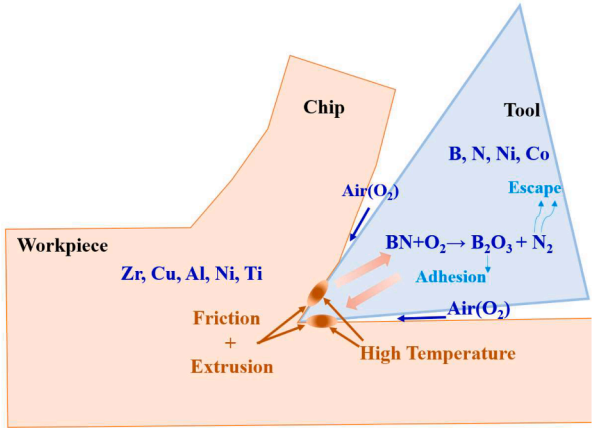

Fig. 7. The chemical reaction process occurred on the rake and flank faces.

investigate the effect of normal stress field distribution on tool wear, the variations of maximum normal stress during machining with different corner radii were calculated.

With an orthogonal cutting mathematical model, the friction angle β and average friction coefficient μ at the tool-chip interface can be expressed by the cutting forces:

$$\beta = \arctan\left(\frac{F_y}{F_z}\right) + \gamma_{oe} \tag{4}$$

$$\mu = \tan\beta \tag{5}$$

where *Fy* is the radial force, *Fz* is the main cutting force and γ_{oe} is the rake angle. The cutting forces, measured during machining, were presented in Fig. 8. It can be seen that the cutting forces increased obviously with the increase of corner radius. The increase of corner radius enhanced the length of cutting edge engaged in cutting, and decreased the actual cutting edge angle, which can enlarge the main cutting force *Fz* and radial force *Fy*, respectively. Based on the calculated results of the friction angle, the shear angle can be calculated by the equation:

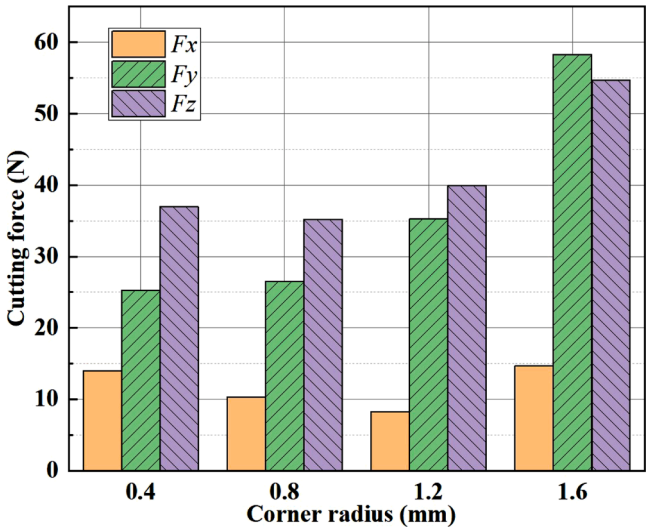

Fig. 8. The cutting force variation with the increase of corner radius.

$$\phi = \frac{\pi}{4} + \frac{\gamma_{oe}}{2} - \frac{\beta}{2}. \tag{6}$$

The change law of shear angle and friction angle during machining Zr-based BMG with different corner radii was presented in Fig. 9. The shear angle decreased with the increase of corner radius, which meant the enlargement of the chip deformation degree. The decrease of shear angle was mainly caused by the increase of friction angle, as shown in Eq. (6). Based on Eq. (4), the friction angle was determined by the ratio of *Fy* to *Fz*. When the tool corner radius increased from 0.4 to 1.6 mm, the radial force *Fy* increased more significantly than the main cutting force *Fz*. In addition, the thickness of the cutting layer decreased with the increase of corner radius, which made the chip deformation easier, leading to a smaller shear angle.

Since the cutting depth a_p was smaller than the corner radius r_ε, the actual cutting edge angle $\kappa_{re}$was influenced by the corner radius, as shown in Fig. 10.According to the geometric relationship, the actual cutting edge angle κ_{re} can be calculated by:

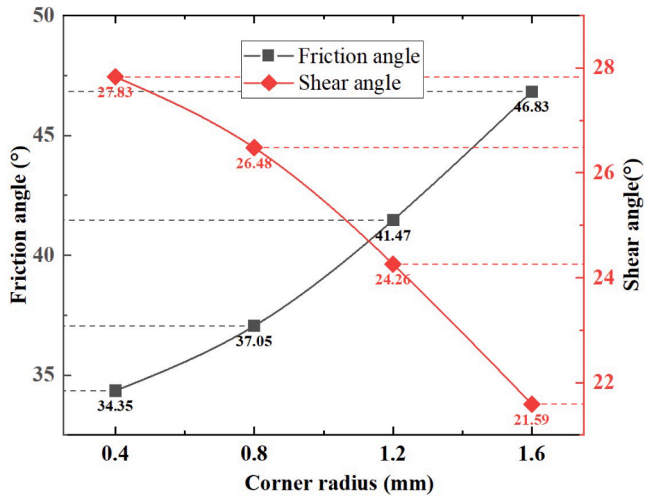

Fig. 9. The variation of shear angle and friction angle with the increase of corner radius.

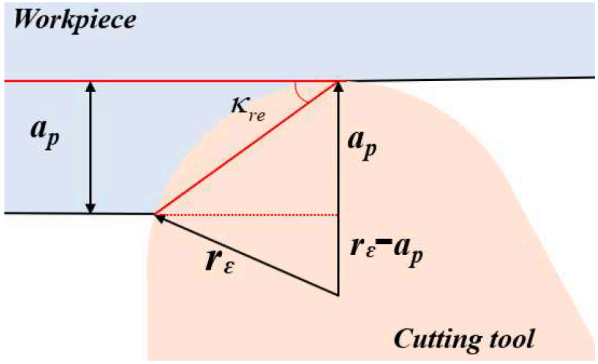

Fig. 10. The actual cutting edge angle calculated with the corner radius.

$$\kappa_{re} = \arctan\left(\frac{a_p}{\sqrt{2a_p r_\varepsilon - a_p^2}}\right). \tag{7}$$

It was obvious that the actual cutting edge angle decreased with the increase of corner radius. The torque of the tool rake face to the chip was:

$$M_{TC} = \int_0^{l_f} \sigma(x)\cdot a_w \cdot x\, dx. \tag{8}$$

Here, l_f is the tool-chip contact length, $\sigma(x)$ is the normal stress, a_w is the cutting width and x is the distance from the tool nose. In addition, the torque of the workpiece material to the chip was:

$$M_{WC} = F_s\cdot\tan(\phi+\beta-\gamma_{oe})\cdot a_t / 2\sin\phi. \tag{9}$$

where F_s is the shear force at the main shear plane, and a_t is the cutting layer thickness. The torques applied to the chip should be balanced as:

$$M_{TC} = M_{WC}. \tag{10}$$

Based on Zorev's assumption, the normal stress on the rake face has the maximum value at the tool nose and decreases gradually along the direction of chip flow. It can be expressed with:

$$\sigma(x) = \sigma_m\left(1-\frac{x}{l_f}\right)^{\eta}. \tag{11}$$

where σ_m is the maximum normal stress at the tool nose, and η is the normal stress decreasing constant. Combining Eqs. (8) and (11), the torque of the tool rake face to the chip can be expressed as:

$$M_{TC} = F_s\cdot\frac{l_f}{\eta+2}\cdot\frac{\cos\beta}{\cos(\phi+\beta-\gamma_{oe})}. \tag{12}$$

Finally, combining Eqs. (9), (10) and (12), the tool-chip contact length can be calculated as [21,22]:

$$l_f = a_t\cdot\frac{\eta+2}{2}\cdot\frac{\sin(\phi+\beta-\gamma_{oe})}{\sin\phi\cdot\cos\beta}. \tag{13}$$

Here, the cutting layer thickness a_t is:

$$a_t = f\cdot\sin\kappa_{re}. \tag{14}$$

According to Eqs. (7), (13) and (14), the theoretical tool-chip contact length l_f can be furtherly expressed with:

$$l_f = f\cdot\sin\left[\arctan\left(\frac{a_p}{\sqrt{2a_p r_\varepsilon - a_p^2}}\right)\right]\cdot\frac{\eta+2}{2}\cdot\frac{\sin(\phi+\beta-\gamma_{oe})}{\sin\phi\cdot\cos\beta}. \tag{15}$$

The cutting width a_w can be expressed with:

$$a_w = \frac{a_p}{\sin\kappa_{re}}. \tag{16}$$

The normal force F_n on the rake face can be calculated with the normal stress integration:

$$F_n = \int_0^{l_f} a_w\cdot\sigma(x)\, dx. \tag{17}$$

It can also be calculated with cutting forces and friction angle:

$$F_n = \sqrt{F_y^2 + F_z^2}\cdot\cos\beta \tag{18}$$

Based on the calculated results of normal force F_n, cutting width a_w and tool-chip contact length l_f, the maximum normal stress σ_m can be obtained by:

$$\sigma_m = \frac{F_n\cdot(\eta+1)}{a_w\cdot l_f}. \tag{19}$$

The calculated results of maximum normal stress with different corner radii are shown in Fig. 11. The maximum normal stress firstly decreased with the corner radius increasing from 0.4 to 1.2 mm, and then increased when the corner radius reached 1.6 mm. The maximum normal stress reached the highest value of 3303 MPa when the corner radius was 0.4 mm. It then decreased to 2868 and 2763 MPa with the corner radius increasing to 0.8 to 1.2 mm, and then increased to 3037

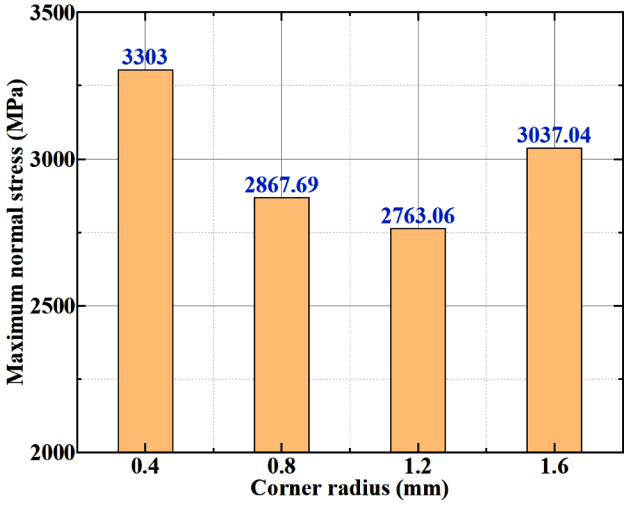

Fig. 11. The calculated results of maximum normal stress at different corner radii.

MPa at the corner radius of 1.6 mm.

Here, the maximum normal stress was mainly influenced by the normal force F_n, the normal stress decreasing constant η and the theoretical tool-chip contact area S can be calculated as:

$$S = a_w \cdot l_f \tag{20}$$

With the increasing of tool corner radius, the normal force F_n increased from 36.95 N to 54.69 N and the theoretical tool-chip contact area S also increased from 0.0447 mm^2 to 0.072 mm^2, as shown in Fig. 12. On the one hand, the increase of normal force F_n enlarged the normal stress at the tool-chip contact area. On the other hand, the increase of theoretical tool-chip contact area S would diminish the normal stress. Therefore, the maximum normal stress σ_m at the tool nose showed a variation trend of decreasing first and then increasing under the combined action of normal force F_n and theoretical tool-chip contact area S. Generally, the edge chipping occurred during machining was usually caused by the excessive local stress. Here, the maximum normal stress at the tool nose was relatively high when the corner radius was 0.4 and 1.6 mm. Then the edge chipping would be easier to occur at this situation, which was also confirmed by the tool wear morphology in previous content.

Considering the entire cutting process, the cutting forces variation during the tool wear process are presented in Fig. 13. With the corner radius of 0.4 mm, the cutting forces increased sharply with the occurrence of serious edge chipping during machining. At the corner radius of 0.8 and 1.2 mm, the tool wear state was improved and built-up edge was found on the cutting edge. With the formation and disappearance of built-up edge, the cutting forces would also show fluctuating changes at this situation. In addition, the resultant cutting force variation, during the tool wear process, was analyzed and the results are shown in Fig. 14. Overall, the resultant cutting force increased with the increase of corner radius. The resultant cutting force also increased obviously with the occurrence of edge chipping when the corner radius was 0.4 mm. As the tool wear process was more stable when the corner radius was 0.8 and 1.2 mm, the variation of resultant cutting force presented a fluctuating trend, which was also caused by the formation and disappearance of built-up edge.

Generally, the stress distribution in cutting area has an important effect on tool wear behavior. An extremely high maximum normal stress may cause the appearance of edge chipping and worsen tool wear state. Moreover, the stress field on rake face is exponentially distributed. The stress near tip is higher and has the greatest effect on tool strength. Therefore, the maximum normal stress can be used as an index of the influence of the tool tip stress field distribution on tool wear. At the corner radius of 0.4 and 1.6 mm, the maximum normal stress is large and the edge chipping is easier to happen at this situation. And the chipping will take away part of the adhesion layer, making it difficult to accumulate on rake face and form BUE. At the same time, the tool wear behavior will also influence the cutting forces during machining. With the formation and disappearance of built-up edge, the variation of cutting forces presented a fluctuating trend.

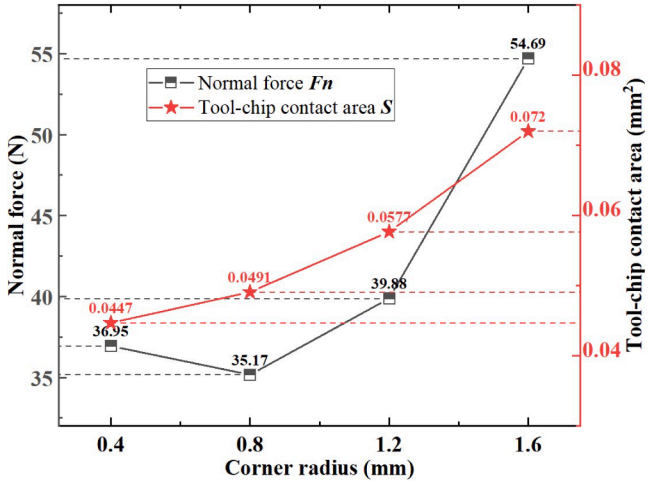

Fig. 12. The variation of normal force F_n and theoretical tool-chip contact area S on the change of corner radius.

3.4. Effect of tool wear behavior on machined surface quality

The machined surface quality is an important factor in evaluating the material machinability. In this work, the machined surface roughness of Zr-based BMGs at different corner radii was investigated. And the surface roughness results with new inserts and worn inserts were compared in Fig. 15. It indicated that the surface roughness with new inserts decreased with the increase of corner radius. According to the theoretical formula of surface roughness, the corner radius and feed rate are the main factors affecting the machined surface roughness. The increase of corner radius will reduce the remain height of machined surface, leading to the improvement of surface roughness.

$$R_a = \frac{0.032 \cdot f^2}{r_\varepsilon} \tag{21}$$

In fact, there are many factors affecting the surface roughness, such as the tool wear state, deformation of machined surface and vibration during machining, other than the remaining height. In order to study the effect of tool wear state on surface roughness, the machined surface roughness after inserts wear is also presented in Fig. 15. The machined surface roughness obtained after inserts wear was almost the same as that obtained after first cut with new inserts when the corner radii were 0.4, 0.8 and 1.2 mm, while it was significantly different when the corner radius was 1.6 mm.

As mentioned above, the tool wear state was different with the variation of corner radius, which also influenced the machined surface roughness. The built-up edge appeared on the cutting edge when the corner radius was 0.8 and 1.2 mm. The edge chipping occurred when the corner radius was 0.4 and 1.6 mm because of the high normal stress. The adhesion on tool rake and flank faces always exist with the corner radius variation. However, the adhesion degree was significantly reduced when the corner radius was 1.6 mm, as presented in Figs. 5 and 6. Here, the edge chipping made the cutting edge become irregular, and the integrity of the machined surface was destroyed. The built-up edge appeared on the cutting edge can lead to local overcutting during machining. With the dynamic formation and disappearance of built-up edge, the cutting depth also changed continuously and the machined surface quality was worsened. Therefore, the appearance of edge chipping and built-up edge both led to the deterioration of surface roughness. Moreover, the adhensions on the flank face reduced the actual tool clearance angle to almost 0°. The extrusion and friction between the tool flank face and workpiece machined surface were intensified. Such almost flat flank face of the tool performed a secondary cutting on the machined surface, and the surface was further finished, as shown in Fig. 16.

Generally, with the corner radius of 0.4, 0.8 and 1.2 mm, although the appearance of edge chipping and built-up edge enlarged the surface roughness, the large amount of adhensions on the tool flank face made the almost flat flank face perform a secondary cutting effect and finish the machined surface. Finally, the surface roughness with worn insert was almost the same as that with new insert. When the corner radius increased to 1.6 mm, only a very small amount of adhensions were found on the tool flank face, as shown in Fig. 5(d). The edge chipping played a dominant role in surface roughness and it destroyed the integrity of cutting edge, leading to the significantly increase of surface roughness.

Furtherly, in order to reveal the relationship between the machined surface quality and tool wear state, the machined surface morphology was analyzed. Fig. 17 presents the machined surface morphology of the

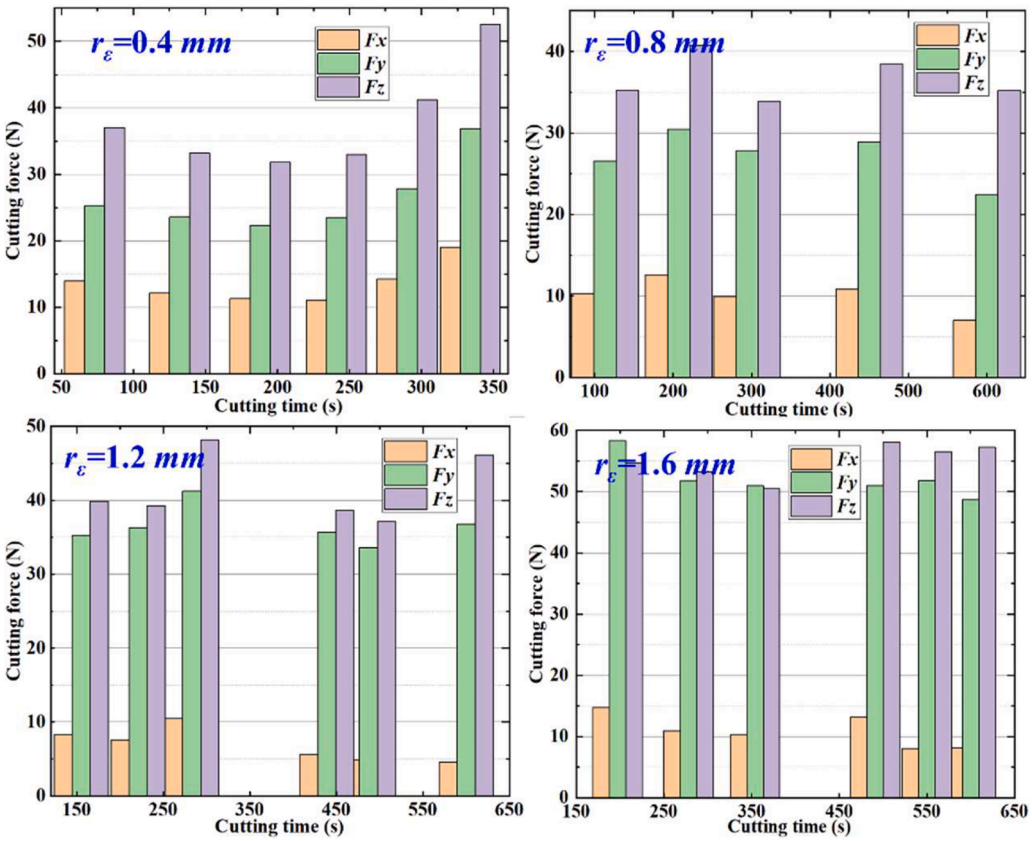

Fig. 13. The variation of cutting forces during the tool wear process.

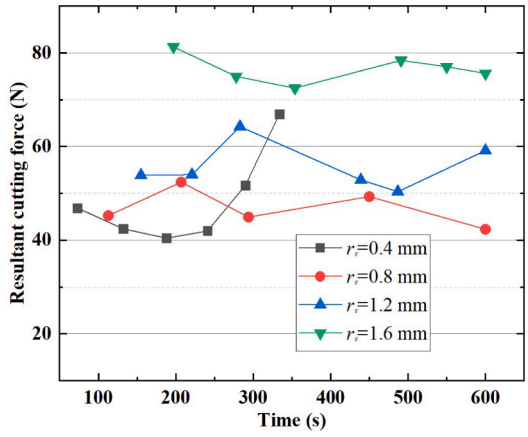

Fig. 14. The resultant cutting force variation during the tool wear process.

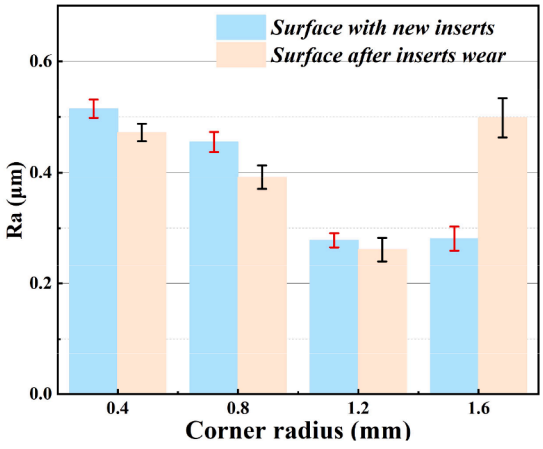

Fig. 15. The machined surface roughness at different corner radii.

Zr-based BMG with different corner radii PCBN tools. It indicated that the machined surface morphology was mainly characterized with feed marks, adhensions and material side flow.

The feed marks were determined by the cutting edge integrity which was influenced by edge chipping. With the appearance of edge chipping, the irregular cutting edge enlarged the extrusion and friction between the tool-workpiece interface. As the low thermal conductivity of workpiece material, local high temperature will soften the workpiece material and form the material side flow during machining. Obvious feed marks were accompanied with material side flow, just as shown in Fig. 17(a) and (d) when corner radius was 0.4 and 1.6 mm.

In addition, adhensions were also found on the machined surface which were come from the debris during machining. The debris on the machined surface were mainly come from the adhensions on the tool rake and flank faces. The debris were bonded to the machined surface under the extrusion action of the tool flank face. The more adhensions on the tool rake and flank faces, the more debris bonded to the machined surface. As presented in Fig. 6, the degree of adhesion decreased obviously with the corner radius increasing from 0.4 to 1.6 mm. The change law was almost the same as that of adhesive wear occurred on the tool rake and flank faces.

In general, the feed marks, adhensions and material side flow all have significant effects on surface quality. Among them, feed marks and material side flow played dominant roles in enlarging surface roughness. Therefore, the surface roughness value with corner radius of 0.4 and 1.6 mm were larger than those with corner radius of 0.8 and 1.2 mm. Considering the adhensions on the machined surface, the degree of

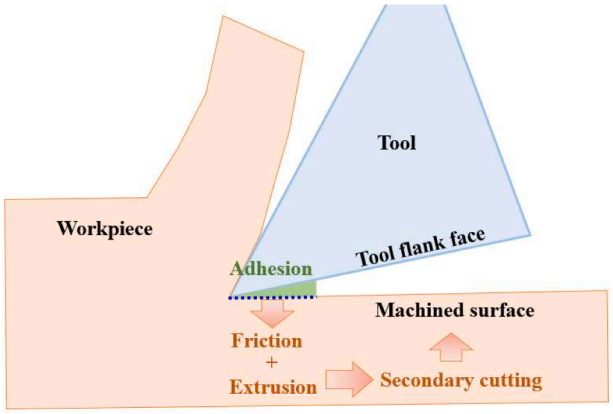

Fig. 16. The extrusion and friction between the tool-workpiece interface.

adhesion with corner radius of 1.2 mm was less than that of 0.8 mm. Finally, the surface roughness had the lowest value at the corner radius of 1.2 mm because of the slight feed marks, material side flow, and adhensions.

Therefore, the relationship between the surface roughness and tool wear state can be related with machined surface morphology. Here, the edge chipping destroyed the integrity of cutting edge and formed feed marks and material side flow on the machined surface, leading to the increase of surface roughness. The adhesive wear, occurred on the tool rake and flank faces, would also produce debris bonded to the machined surface, forming adhensions and enlarging surface roughness.

Amorphous atomic characteristics are the reason for the excellent mechanical properties of Zr-based BMG. However, the high temperature in the cutting area may cause machined surface material crystallization due to the increased tool wear during cutting process and the extremely low thermal conductivity of BMG. Therefore, the machined surfaces of Zr-based BMG at different corner radii were detected with XRD diffraction analysis as shown in Fig. 18. The results show that there is no obvious sharp crystal diffraction peak on the machined surfaces. It indicates that the amorphous characteristics of Zr-based BMG have no change during the cutting process.

4. Conclusions

In summary, the tool wear mechanisms of machining Zr-based BMGs with PCBN tools were investigated. The corner radius had a significant influence on the tool wear behavior during machining. The tool wear state was relatively stable when the corner radius was 0.8 and 1.2 mm, with the appearance of built-up edge. A smaller or larger corner radius would both lead to edge chipping because of the stress concentration and the impact of shock and vibration during machining. Adhesive and oxidation wear are the main wear mechanisms during machining Zr-based BMGs with PCBN tools. Due to the low thermal conductivity of workpiece material, the high cutting temperature caused the CBN particles in the tool material and Co element in the binder to react with oxygen in air, leading to oxidation wear.

Furtherly, the tool wear mechanism was significantly affected by the normal stress field distribution. With the increase of corner radius, the maximum normal stress at the tool nose showed a variation trend of decreasing first and then increasing under the combined action of normal force F_n and theoretical tool-chip contact area S. The high maximum normal stress was the main reason for edge chipping. The relationship between the surface roughness and tool wear state was related to the machined surface morphology. The edge chipping destroyed the integrity of cutting edge, forming feed marks and material side flow on the machined surface, and leading to the increase of surface roughness. The secondary cutting and finish on the machined surface by flank face adhensions can reduce the increase in surface roughness caused by adhesive debris on the machined surface. Finally, the surface roughness should be the result of the combined action of these factors.

CRediT authorship contribution statement

Junsheng Zhang: Conceptualization, Methodology, Validation, Writing – original draft, Writing – review & editing. **Rang Li:** Methodology, Validation, Data curation. **Libao Zhang:** Methodology,

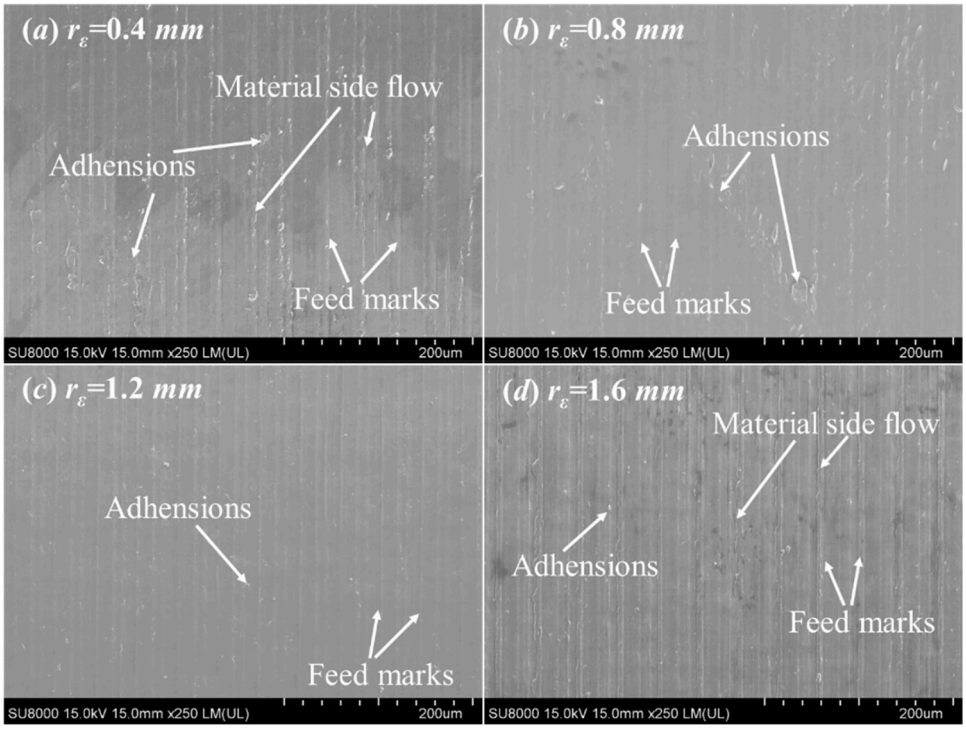

Fig. 17. The machined surface morphology of Zr-based BMG.

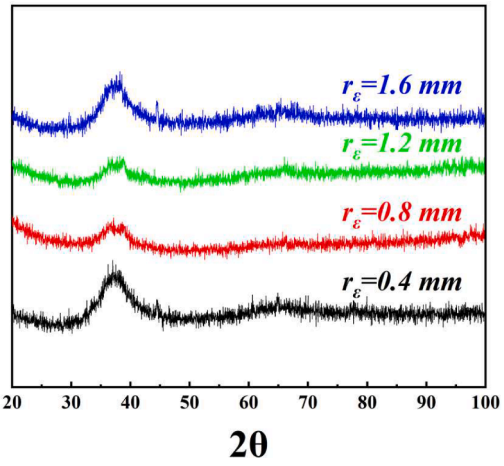

Fig. 18. XRD patterns of the machined surfaces of Zr-based BMG at different corner radii.

Validation, Data curation. **Haidong Yang:** Conceptualization, Methodology, Validation. **Huohong Tang:** Writing – review & editing. **Shunhua Chen:** Conceptualization, Validation, Writing – review & editing, Supervision.

Declaration of Competing Interest

The authors declare that they have no known competing financial interests or personal relationships that could have appeared to influence the work reported in this paper.

Data availability

Data will be made available on request.

Acknowledgments

This work was mainly supported by the Anhui Provincial Natural Science Foundation (Grant No. 2108085ME171) and the Fundamental Research Funds for the Central Universities of China (Grant No's. PA2023GDSK0075 and JZ2022HGTB0247).

References

[1] S.H. Chen, Q. Ge, J.S. Zhang, W.J. Chang, J.C. Zhang, H.H. Tang, H.D. Yang, Low-speed machining of a Zr-based bulk metallic glass, J. Manuf. Process 72 (2021) 565–581, https://doi.org/10.1016/j.jmapro.2021.10.055.
[2] Z.X. Huo, G.Q. Zhang, J.H. Han, J.P. Wang, S. Ma, H.T. Wang, A review of the preparation, machining performance, and application of Fe-based amorphous alloys, Processes 10 (2022) 1203, https://doi.org/10.3390/pr10061203.
[3] Z.J. Zhao, S. To, J.W. Wang, G.Q. Zhang, Z.M. Weng, A review of micro/nanostructure effects on the machining of metallic materials, Mater. Des. 224 (2022), 111315, https://doi.org/10.1016/j.matdes.2022.111315.
[4] M. Bakkal, A.J. Shih, R.O. Scattergood, Chip formation, cutting forces, and tool wear in turning of Zr-based bulk metallic glass, Int. J. Mach. Tools Manuf. 44 (2004) 915–925, https://doi.org/10.1016/j.ijmachtools.2004.02.002.
[5] M. Wang, B.S. Xu, J.Y. Zhang, S.Y. Dong, S.C. Wei, Experimental observations on surface roughness, chip morphology, and tool wear behavior in machining Fe-based amorphous alloy overlay for remanufacture, Int. J. Adv. Manuf. Technol. 67 (2013) 1537–1548, https://doi.org/10.1007/s00170-012-4588-z.
[6] X. Chen, J.F. Xiao, Y. Zhu, R.J. Tian, X.W. Shu, J.F. Xu, Micro-machinability of bulk metallic glass in ultra-precision cutting, Mater. Des. 136 (2017) 1–12, https://doi.org/10.1016/j.matdes.2017.09.049.
[7] J. Xiong, H. Wang, G.Q. Zhang, Y.B. Chen, J. Ma, R.D. Mo, Machinability and surface generation of $Pd_{40}Ni_{10}Cu_{30}P_{20}$ bulk metallic glass in single-point diamond turning, Micromachines 11 (2020) 4, https://doi.org/10.3390/mi11010004.
[8] Y. Deng, C.Y. Wang, F. Ding, T. Zhang, W.K. Wu, Thermo-mechanical coupled flow behavior evolution of Zr-based bulk metallic glass, Intermetallics 152 (2023), 107770, https://doi.org/10.1016/j.intermet.2022.107770.
[9] M. Bakkal, A.J. Shih, S.B. McSpadden, R.O. Scattergood, Thrust force, torque, and tool wear in drilling the bulk metallic glass, Int. J. Mach. Tools Manuf. 45 (2005) 863–872, https://doi.org/10.1016/j.ijmachtools.2004.11.005.
[10] F. Ding, C.Y. Wang, T. Zhang, Q. Zhao, L.J. Zheng, Light emission of Zr-based bulk metallic glass during high-speed cutting: from generation mechanism to control strategies, J. Mater. Process. Technol. 305 (2022), 117598, https://doi.org/10.1016/j.jmatprotec.2022.117598.
[11] N.K. Maroju, D.P. Yan, B.Y. Xie, X.L. Jin, Investigations on surface microstructure in high-speed milling of Zr-based bulk metallic glass, J. Manuf. Process. 35 (2018) 40–50, https://doi.org/10.1016/j.jmapro.2018.07.020.
[12] T. Wang, X.Y. Wu, G.Q. Zhang, B. Xu, Y.H. Chen, S.C. Ruan, Experimental study on machinability of Zr-based bulk metallic glass during micro milling, Micromachines 11 (2020) 86, https://doi.org/10.3390/mi11010086.
[13] Z.M. Chen, P.F. Feng, J.J. Wang, F. Feng, H.T. Zha, Understanding the abnormal effects of ultrasonic vibration on tool wear and surface generation in Zr-based bulk metallic glass cutting, CIRP J. Manuf. Sci. Technol. 39 (2022) 1–17, https://doi.org/10.1016/j.cirpj.2022.07.004.
[14] Z.A.M. Tagiuri, T.M. Dao, A.M. Samuel, V. Songmene, A numerical model for predicting the effect of tool nose radius on machining process performance during orthogonal cutting of AISI 1045 steel, Materials 15 (2022) 3369, https://doi.org/10.3390/ma15093369.
[15] K.Y. Lin, W.H. Wang, R.S. Jiang, Y.F. Xiong, Effect of tool nose radius and tool wear on residual stresses distribution while turning *in situ* TiB_2/7050 Al metal matrix composites, Int. J. Adv. Manuf. Technol. 100 (2019) 143–151, https://doi.org/10.1007/s00170-018-2742-y.
[16] U. Umer, A. Al-Ahmari, 3D modeling of tool wear and optimization in hard turning considering the effects of tool cutting edge and nose radii, Int. J. Adv. Manuf. Technol. 118 (2022) 1919–1932, https://doi.org/10.1007/s00170-021-07998-0.
[17] H.D. Yang, Y.S. Wu, J.S. Zhang, H.H. Tang, W.J. Chang, J.C. Zhang, S.H. Chen, Study on the cutting characteristics of high-speed machining Zr-based bulk metallic glass, Int. J. Adv. Manuf. Technol. 119 (2022) 3533–3544, https://doi.org/10.1007/s00170-021-08630-x.
[18] H.D. Yang, L.B. Zhang, J.S. Zhang, H.H. Tang, S.H. Chen, Effect of sample size and cooling rate on the plastic deformation behavior of bulk metallic glasses: a comparative study, J. Non Cryst. Solids 589 (2022), 121643, https://doi.org/10.1016/j.jnoncrysol.2022.121643.
[19] Y.Q. Liu, L. Liu, P.F. Shi, Y. Wang, L.M. Qian, L. Chen, Improved wear resistance of CBN tool enabled by hBN as a water-based lubricant additive through suppressing tribochemical reactions, Ceram. Int. 49 (2023) 17953–17960, https://doi.org/10.1016/j.ceramint.2023.02.164.
[20] Z. Liu, Y.J. Gong, W. Zhou, L.L. Ma, J.J. Yu, J.C. Idrobo, J. Jung, A.H. MacDonald, R. Vajtai, J. Lou, P.M. Ajayan, Ultrathin high-temperature oxidation-resistant coatings of hexagonal boron nitride, Nat. Commun. 4 (2013) 2541, https://doi.org/10.1038/ncomms3541.
[21] J.S. Zhang, H.D. Yang, H.H. Tang, S.H. Chen, Study on the tool life analysis for free-cutting steels, Proc. Inst. Mech. Eng. Part B J. Eng. Manuf. 236 (2022) 1706–1715, https://doi.org/10.1177/09544054221080038.
[22] J.S. Zhang, Y.S. Shang, H.D. Yang, H.H. Tang, S.H. Chen, On the stress field redistribution of tool–chip interface for micro-groove textured tools, Int. J. Adv. Manuf. Technol. 126 (2023) 4637–4650, https://doi.org/10.1007/s00170-023-11461-7.